Journal of Molecular Catalysis A: Chemical 394 (2014) 151–161

Contents lists available at ScienceDirect

Journal of Molecular Catalysis A: Chemical

journal homepage: www.elsevier.com/locate/molcata

Evaluating Pd–Ni layered catalysts for selective hydrogenation of 1,3-butadiene: A theoretical perspective

Guillermina Gómez, Patricia G. Belelli*, Gabriela F. Cabeza, Norberto J. Castellani

Grupo de Materiales y Sistemas Catalíticos, Departamento de Física (IFISUR) Universidad Nacional del Sur, Av. Alem 1253, Bahía Blanca B8000CP, Argentina

ARTICLE INFO

Article history:
Received 13 August 2013
Received in revised form 24 June 2014
Accepted 30 June 2014
Available online 5 July 2014

Keywords:
1,3-Butadiene
Partial hydrogenation
Pd–Ni surfaces
Periodic DFT

ABSTRACT

The partial hydrogenation of 1,3-butadiene (13BD) to several C_4H_8 products, including 1-butene (1B), 2-butene (2B) and butan-1,3-diyl (B13R), on both Pd/Ni(1 1 1) and Pd_3/Ni(1 1 1) bimetallic surfaces was theoretically investigated using DFT methods. For that purpose, different intermediates C_4H_7 and C_4H_8 radical species were evaluated according to the Horiuti–Polanyi mechanism performed in two sequential steps. The whole process was found to be exothermic on Pd/Ni(1 1 1) and endothermic on Pd_3/Ni(1 1 1). Furthermore, the former surface, where the intermediate adsorptions are more favorable, exhibits lower activation barriers than Pd_3/Ni(1 1 1). On both surfaces, the B13R formation is associated with high transition state energies through the pathways studied here; for this reason, it is extremely improbable to obtain B13R. Our calculations predict that on the Pd/Ni(1 1 1) catalyst model, the products would be mainly the butene isomers, with a little more selectivity toward 2B, in contrast to the pure Pd surface and in agreement with experimental data.

1. Introduction

1,3-Butadiene (13BD) is the simplest alkene containing conjugated bonds, that is why it can be considered as a model molecule to study the factors controlling the activity and selectivity in partial hydrogenation over a catalyst. In particular, the selective hydrogenation of 13BD is not only an important reaction in the purification of light alkenes in polymerization processing [1], but also it is a good prototype in probing the catalytic properties and electronic structures of metal catalysts [2,3]. Specifically, if we know what controls selectivity toward the formation of *cis* versus *trans* olefins [4], it will have significant practical applications; for instance, it is desirable to reduce the production of *trans* fatty acids during the partial hydrogenation of natural oils to edible fats [5]. However, hydrogenation will lead to either *trans*- or *cis*-2-butene products since there are *trans*- and *cis*-isomers in the 1,3-butadiene molecule.

The Pd and Pt metallic systems have been the focus of most studies because they play a great role in heterogeneous catalysis devoted to hydrogenation. In the last few years, the developments in the field of computational chemistry have made feasible the theoretical investigations of realistic catalytic systems. Thus, the adsorption of representative molecules such as ethylene, propylene, butadiene, etc, on these surfaces has been covered with a large range of experimental techniques (such as LEED, EELS, STM, or TPD) [6–8] as well as theoretical calculations [9–13].

Specifically, in experimental studies carried out on Pt(1 1 1) surface by Lee et al. [14], the selectivity for *cis*/*trans*-2-butene isomerization was investigated by measuring their kinetics in the presence of a small amount of hydrogen. The corresponding results indicated that the *trans*-2-butene isomerization to its *cis* isomer is easier than the opposite *cis*-to-*trans* conversion on Pt(1 1 1) single-crystal surface. The kinetic study on the butene catalytic conversion also suggested different selectivities on Pt(1 1 1) and Pt(1 0 0) surfaces. In a further study, the ratios of *trans*-to-*cis* vs. *cis*-to-*trans* conversion rates on both tetrahedral and cubic supported Pt particles as a function of the temperature were investigated [15]. Results show that the selectivity of the reaction may be controlled by using supported catalysts with appropriate metal particle shapes. Pd deposited on Ni(1 1 1) is an interesting catalytic situation to study for the 1,3-butadiene hydrogenation is when. In previous experimental work [16], the very poor activity of Ni(1 1 1) surface ($\sim 10^{14}$ molecules converted/cm^2 s at 300 K and under P_{H_2} = 35 Torr) evidenced a strong increase after deposition of 0.5 ML Pd at 300 K under UHV conditions, reaching an average value between Pd(1 1 1) and Pd(1 1 0) activities ($\sim 10^{15}$ mol/cm^2 s). Selectivity ratio toward butene isomers always remained close to unity.

* Corresponding author. Tel.: +54 291 4595141; fax: +54 291 4595142.
E-mail address: patricia.belelli@uns.edu.ar (P.G. Belelli).

http://dx.doi.org/10.1016/j.molcata.2014.06.035
1381-1169/

Based on these previous results, the Pd–Ni system was brought to our attention. Firstly, the study of the structural, electronic and magnetic properties of multilayer bimetallic systems Pd_n/Ni(1 1 1), with $n = 0$ to 4 Pd layers over a Ni(1 1 1) substrate, was performed [17]; and then the 13BD adsorption on Pd/Ni(1 1 1) and Pd_3/Ni(1 1 1) surfaces were rigorously evaluated [18].

In the present theoretical approach, the partial hydrogenation of 1,3-butadiene (13BD) to several C_4H_8 species on both Pd/Ni(1 1 1) and Pd_3/Ni(1 1 1) bimetallic surfaces using DFT methods is further investigated. This study is organized as follows: Section 2 gives an overview of the methodology used; in Section 3, the adsorption structures and relative stabilities of different intermediates (C_4H_7 and C_4H_8 radical species) are examined; specifically, the possible reaction pathways of 13BD partial hydrogenation performed on both metal surfaces are presented in Section 3.3. Finally, the conclusions are drawn in Section 4.

2. Computational details and surface models

The calculations reported in this work were carried out in the framework of density functional theory (DFT) using the Vienna ab initio simulations package (VASP) [19–21]. Electron exchange and correlation effects are described by the generalized gradient approximation (GGA) using the functional proposed by Perdew–Wang (PW91) [22,23]. The Kohn–Sham one-electron wave functions were expanded on the basis of plane waves with kinetic energy below 450 eV. A $(3 \times 3 \times 1)$ Monkhorst–Pack grid of special k points was adopted for integration in the reciprocal space. The projector augmented wave (PAW) method developed by Blochl [24] was used to reproduce the atomic core effects in the electronic density of the valence electrons. The PAW is essentially an all-electron frozen core method combining the accuracy of all electron methods, such as the full potential linearized plane wave method, and the computational simplicity of the pseudopotential approach, especially in the implementation of Kresse and Joubert [25]. The Methfessel–Paxton method [26] with a smearing width of 0.20 eV was used to determine how the partial occupancies are set for each one-electron wave function. The calculations were performed at the spin polarized level to take into account the magnetic properties of the systems.

For all the calculations, a FCC stacking layered structure was assumed. The (1 1 1) metallic surfaces were represented with a slab containing four layers of atoms separated in the normal direction by a vacuum region. The width of this gap was optimized to avoid the interaction between slabs. For that purpose, we observed that a distance of ~15 Å is adequate. Our investigations were focused in the 13BD partial hydrogenation on two multilayered bimetallic surfaces Pdn/Ni(1 1 1) with $n = 1$ and 3 Pd layers over a Ni(1 1 1) substrate, i.e. Pd/Ni(1 1 1) and Pd3/Ni(1 1 1), respectively. The structural, electronic and magnetic properties of both surfaces were previously analyzed considering the ferromagnetic condition acquired by the Pd overlayer epitaxially deposited on the Ni(1 1 1) surface [17]. For Pd/Ni(1 1 1) and Pd_3/Ni(1 1 1), the Pd–Pd interatomic distances in the first layer were optimized to 2.57 Å and 2.75 Å, respectively.

The hydrogenation of 1,3-butadiene (13BD) can lead to different products: partial hydrogenation yields to butene, while total hydrogenation leads to butane. The Horiuti-Polanyi mechanism [27,28] implies the initial formation of a C_4H_7 moiety and its subsequent hydrogenation to a C_4H_8 species. The determination of the transition state energies (ΔE_{TS}) and the activation barriers were performed by the nudged elastic band method (NEB) [29]. This method, as implemented in VASP, allows finding the minimum energy path of reaction and the transition state (TS). The validity of transition states so obtained was checked by a full vibrational frequency analysis, achieved by calculating the Hessian matrix, followed by a diagonalization procedure to obtain the eigenmodes. The corresponding transition states present only one negative force constant. Then, we checked that the eigenvector associated with this negative force constant was related to the reaction pathway considered. This procedure allows us to obtain accurate transition states energies and activation barriers.

Relative reaction energies (E_{rel}) taking both isolated 13BD $\left(E_{C_4H_6(g)}\right)$ and H_2 $\left(E_{H_2(g)}\right)$ molecules in gas phase as energy references were calculated according to the equation:

$$E_{rel} = E_{C_4H_x/surf} + (8 - x)E_{H/surf} - (9 - x)E_{surf} - E_{C_4H_6(g)} - E_{H_2(g)} \quad (1)$$

where C_4H_x corresponds to 13BD, to 13BD in co-adsorption with H, to one of the possible intermediates as well as to the latter in co-adsorption with another H; $E_{H/surf}$ is the adsorption energy of an isolated hydrogen atom, E_{surf} is the energy of bare surface and x is the amount of H atoms in the reaction ($x = 6,7,8$). The corresponding adsorption energies were calculated as the difference between the energy of the adsorbed molecule on the surface and the sum of the bare surface (E_{surf}) and the gas phase molecule energies. A negative value indicates an exothermic chemisorption process. A large box of $(20 \times 20 \times 20)$ Å^3 was used to obtain the gas phase molecule energy. The binding site preference and the adsorption energies of 13BD on both bimetallic surfaces were already published [18]. The geometries of adsorbates together with the two uppermost layers of the surface were fully optimized.

Energy profiles associated with the reaction pathways were plotted from the reactants to provide the products adsorbed on the surface, assuming certain energy as zero reference. In our case, this reference corresponds to the sum of the energies of 13BD and two H atoms adsorbed at infinite distance (without interaction). Non-zero-point-energy (ZPE) corrections were made because it was found that the ZPE contributions to relative reaction energies and the activation energies were below 0.01 eV.

3. Results and discussion

In a previous work we proved theoretically that the most stable adsorption mode for 13BD on Pd/Ni(1 1 1) and Pd_3/Ni(1 1 1) surfaces is the 1,2,3,4-tetra-σ one [18]. 13BD shows in this geometry the *trans* configuration, with each of their four C atoms linked to a different surface Pd atom through a σ-bond. From this result, in the present paper the 13BD hydrogenation on both surfaces was considered following the Horiuti-Polanyi mechanism, where the co-adsorbed H atom is added into one of the C=C double bonds of the 13BD to produce two C_4H_7 intermediates: 1-buten-4-yl ($CH_2{=}CHCH_2CH_2\bullet$, 1B4R) and 2-buten-1-yl ($CH_2\bullet CH{=}CHCH_3$, 2B1R), which are formed by H addition on the C_2 (or C_3) and C_1 (or C_4), respectively. The subsequent incorporation of another H atom produces the C_4H_6 products: 1-butene (1B), 2-butene (2B) and the diradicals butan-1,3-diyl (B13R) and butan-1,4-diyl (B14R) [30]. Taking into account the different steps necessary to describe reaction pathways in the Horiuti–Polanyi mechanism, we present in following subsections first the intermediate species (1B4R and 2B1R), afterward, the co-adsorptions (13BD + H, 1B4R + H and 2B1R + H), and finally the reaction pathways and transition states.

3.1. Intermediate species on Pd/Ni(1 1 1) and Pd_3/Ni(1 1 1) surfaces

Figs. 1 and 2 show the optimized geometries of the intermediate species on Pd/Ni(1 1 1) and Pd_3/Ni(1 1 1), respectively. Both monoradicals produced after the first hydrogenation, 1B4R and 2B1R, have the C = C double bonds lengthened with respect to the free diene in gas phase (1.34 Å) and the Pd—C bonds also change

Table 1
Relative reaction energies (E_{rel} in eV) and the most relevant geometrical parameters (expressed in Å) of the C_4H_x (x = 7 and 8) adsorbed on Pd/Ni(1 1 1) and Pd_3/Ni(1 1 1). The corresponding geometries of the 13BD adsorbed on 1,2,3,4-tetra-σ site are also presented.

Surface	Species	E_{rel}	C_1–C_2	C_2–C_3	C_3–C_4	Pd–C_1	Pd–C_2	Pd–C_3	Pd–C_4
Pd/Ni(1 1 1)	1B4R	−0.96	1.43	1.52	1.52	2.17	2.21	–	2.08
	2B1R	−1.35	1.43	1.42	1.51	2.20	2.58	2.14	–
	B13R	−1.14	1.51	1.52	1.51	2.09	–	2.08	–
	B14R	−0.96	1.52	1.54	1.52	2.08	–	–	2.08
	13BD	−1.04	1.43	1.43	1.43	2.16	2.34	2.43	2.16
	1B	−1.69	1.44	1.51	1.54	2.16	2.14	–	–
	2B	−1.64	1.52	1.45	1.52	–	2.16	2.16	–
Pd_3/Ni(1 1 1)	1B4R	−0.84	1.45	1.52	1.52	2.14	2.16	–	2.07
	2B1R	−1.16	1.44	1.43	1.51	2.11	2.61	2.18	–
	B13R	−0.45	1.51	1.51	1.52	2.07	–	2.11	–
	B14R	−0.30	1.52	1.54	1.52	2.09	–	–	2.08
	13BD	−1.53	1.45	1.45	1.43	2.10	2.22	2.29	2.10
	1B	−0.98	1.45	1.52	1.54	2.12	2.16	–	–
	2B	−0.95	1.52	1.46	1.51	–	2.14	2.12	–

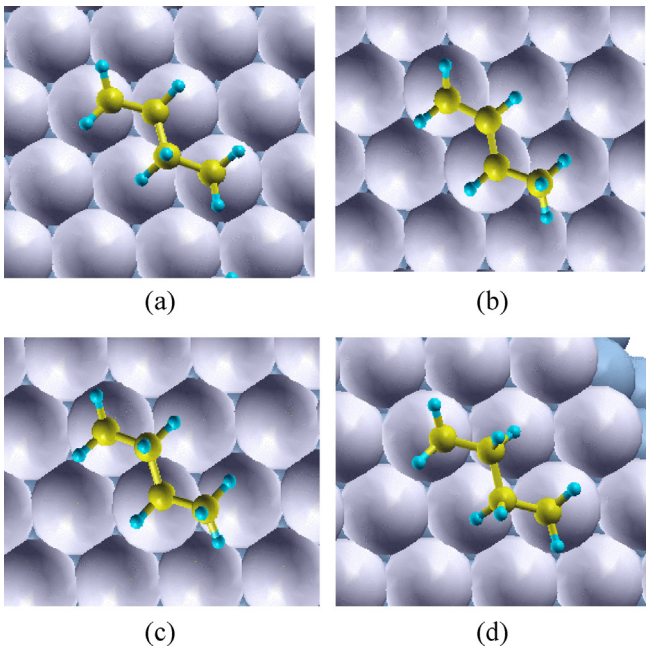

Fig. 1. Adsorption modes of (a) 1-buten-4-yl (1B4R), (b) 2-buten-1-yl (2B1R) and (c) butan-1,3-diyl (B13R) and (d) butan-1,4-diyl (B14R) on Pd/Ni(1 1 1). Pd atoms are in gray, C atoms in yellow and the H atoms in cyan.

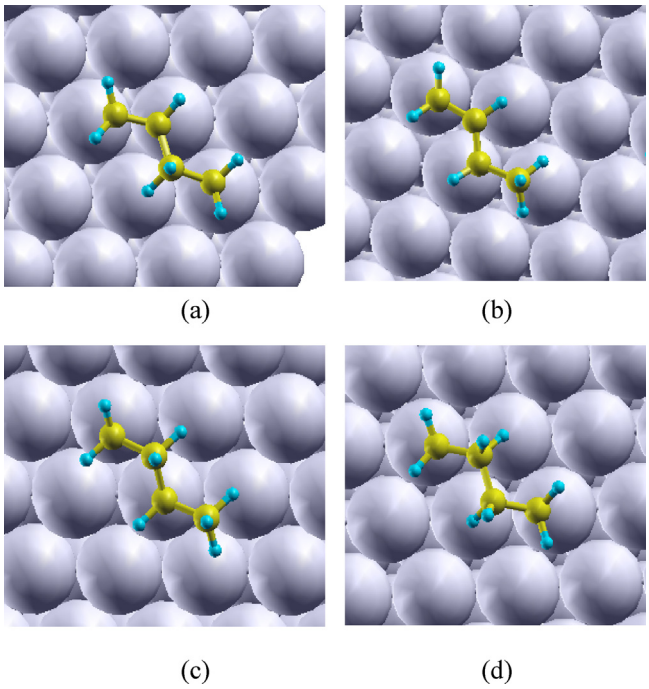

Fig. 2. Adsorption modes of (a) 1-buten-4-yl (1B4R), (b) 2-buten-1-yl (2B1R) and (c) butan-1,3-diyl (B13R) and (d) butan-1,4-diyl (B14R) on Pd_3/Ni(1 1 1).

with respect to the adsorbed 13BD molecule (Table 1). In case of 2B1R intermediate, the C_2—C_3 bond is shorter than a C—C single bond and similarly to the C_1—C_2 bond, indicating that this species has allylic character. Comparing the 2B1R adsorption geometry on Pd/Ni(1 1 1) with respect to Pd_3/Ni(1 1 1) and other surfaces, as Pd(1 1 1) and Pt(1 1 1) [30], we observe that the C_1—C_2 and C_2—C_3 bonds are slightly shorter on the first surface; therefore, 2B1R shows a higher allylic character on Pd/Ni(1 1 1) than on the other surfaces.

Besides, Pd—C bonds for 2B1R and 1B4R intermediates change with respect to adsorbed 13BD molecule. In particular, the Pd—C_2 bond for 2B1R on both bimetallic systems is more lengthened. Furthermore, we note that the Pd—C distances are mainly dependent on the type of surface and on the length of radical C—C bonds. When the radical has short C_1—C_2 and C_2—C_3 bonds (about 1.43 Å), as 2B1R radical, Pd–C distances are shorter on Pd/Ni(1 1 1) than on Pd_3/Ni(1 1 1). On the other hand, if the radical has long C—C bonds (about 1.43 and 1.52 Å), as 1B4R, then Pd–C distances are longer on Pd/Ni(1 1 1) than on Pd_3/Ni(1 1 1). The more open structure of Pd_3/Ni(1 1 1) in comparison with Pd/Ni(1 1 1) (Pd—Pd distances of 2.57 Å and 2.75 Å, respectively) improves the anchoring of molecules with long C—C bonds.

In order to compare the adsorption stability of these radicals, we calculate the relative reaction energy, E_{rel}, defined previously in Eq. (1). From the results summarized in Table 1, it is possible to observe the higher stability of 2B1R radical with respect to 1B4R radical on both Pd–Ni surfaces, with an E_{rel} difference of at least 0.39 eV between the adsorbed radicals. The most significant stability of 2B1R can be clearly associated with its allylic character.

In the second hydrogenation step, two different species, B13R and B14R diradicals, can also be obtained. The only difference between them is established by the location of the radical within the carbon chain. All C—C bonds are in the length range of 1.51–1.54 Å, thus indicating the sp^3 hybridization of their four C atoms. They are C_4H_8 species, as the butene isomers; consequently, the comparison of their E_{rel} values is a way to understand the reaction process. In particular, B14R adsorbed on Pd/Ni(1 1 1) is more unstable than the B13R species (0.18 eV), but its instability is more pronounced when it is compared with 1B, giving an E_{rel} difference of 0.73 eV (and 0.55 eV for B13R). The role played by B14R

diradical was not taken into account in this study due to its lowest stability among the different possible C_4H_8 species. Regarding the Pd_3/Ni(1 1 1) surface, all the C_4 species show the same behavior just outlined for the Pd/Ni(1 1 1) surface.

3.2. Co-adsorptions C_4H_x and H atom on Pd/Ni(1 1 1) and Pd_3/Ni(1 1 1) surfaces

In this subsection we analyze the co-adsorption of a H atom and C_4H_x (x = 6 or 7) species, i.e. 13BD, 1B4R and 2B1R on Pd/Ni(1 1 1) and Pd_3/Ni(1 1 1). On both surfaces, the most stable H adsorption site is the 3-fold *fcc* hollow site, in agreement with other works [30–34]. Thus initially, H adsorption was placed in different hollow *fcc* positions, vicinal to the C atom to hydrogenate.

Several co-adsorption configurations were evaluated for H and different C_4H_x species, but only the most stable were selected in each case to build the reaction pathways (Table 2). On Pd/Ni(1 1 1), the H position changes after geometry optimization from a hollow site to pseudo-bridge site neighboring the C atom to be hydrogenated. Something similar occurs on Pd_3/Ni(1 1 1). The z coordinate of this co-adsorbed H atom measured from the surface is about 1.0 Å, which is also reported for H atom adsorbed on bridge sites of other surfaces [35]. This behavior can be related to the fact that both H and C_4H_x species share the same Pd atom on the surface, as well as the higher H mobility on metallic surfaces like Pd(1 1 1) and Pt(1 1 1) [10,36]. Similar results were found by Neurock and van Santen [12], when they studied the co-adsorption of H and ethylene on Pd(1 1 1) and by Válcarcel et al. [30] for the co-adsorption of H and 13BD on Pt(1 1 1) and Pd(1 1 1).

On both Pd–Ni surfaces, no significant changes of the C—C bonds for 13BD and 1B4R are present in the co-adsorptions with H, compared to their corresponding geometries as isolated adsorbed species. Nevertheless, the adsorbed H atom near the C_3 atom of the 13BD molecule produces the Pd—C_3 bond stretching of 0.1 Å, showing the steric repulsion between the adsorbates. When H is co-adsorbed near the C_1 or C_3 of the 2B1R radical, we note that the C_1—C_2 and C_2—C_3 bonds suffer a shortening and a stretching, 1.41 Å and 1.44 Å, regarding the C—C bonds in the isolated adsorbed 2B1R, 1.43 Å and 1.42 Å, respectively. Although these changes seem to be small, they are significant due to the allylic character of 2B1R species (•C_1—C_2=C_3).

For comparison purposes, E_{rel} of these co-adsorptions were calculated (Table 2), with respect to the 13BD molecule and H atom independently adsorbed on Pd/Ni(1 1 1) and Pd_3/Ni(1 1 1). The values of other energetic parameters, ΔE_{int}, that measures the lateral interaction of the co-adsorbed species, were also summarized in Table 2. They were calculated through the following equation:

$$\Delta E_{int} = E_{rel(C_4H_x+H)/surf} - E_{rel(C_4H_x/surf)} - E_{rel(H/surf)} \quad (2)$$

where $E_{rel(C_4H_x+H)/surf}$ is the E_{rel} of the co-adsorbed species C_4H_x and H. The $E_{rel(C_4H_x+H)/surf}$ and $E_{rel(H/surf)}$ are the E_{rel} values for the same species, adsorbed independently of each other (see Table 1).

In general, the co-adsorptions on the bimetallic surfaces studied here produce instability of the systems, giving positive ΔE_{int} values in the ~0.10–0.30 eV range. These results are in agreement with those obtained for ethylene [12], acetylene [11] and 13BD [30] adsorbed on different metallic surfaces, during the hydrogenation reaction. In particular, the co-adsorption of 2B1R and H (near to C_1) on Pd/Ni(1 1 1) is the only case where there is no repulsion, probable due to the longer distance between the co-adsorbates, 2.80 Å, in relation to the remaining cases, 2.50 Å. The highest repulsive interaction was observed for the H co-adsorbed near the C_3 of 2B1R on Pd_3/Ni(1 1 1). We note that ΔE_{int} values are high both when the C_4H_x species co-adsorbed with H on Pd/Ni(1 1 1) have long C—C bonds (like 13BD and 1B4R radical) and when the C_4H_x species co-adsorbed with H on Pd_3/Ni(1 1 1) have short C—C bonds (like 2B1R radical). This behavior can be related with the relative stabilities previously mentioned in Section 3.1.

3.3. Reaction pathways for the 13BD partial hydrogenation

3.3.1. On Pd/Ni(1 1 1)

The geometries of the transition states (TS) are basically formed by a three centre structure (Pd—C—H), when the co-adsorbed H atom begins to bind with C atom of the 13BD, whereas the Pd—H and Pd—C bonds begin to break. Table 3 summarizes the most important geometrical parameters and the transition state energies on Pd/Ni(1 1 1). In the first step through 1B4R radical, the C—H distance of TS is reduced from 2.76 Å (co-adsorption state) to 1.68 Å in the TS (Fig. 3a). In the same way, Pd—C bond increases from 2.55 Å to 2.82 Å. In the TS geometry toward 2B1R, the C—H distance is slightly shorter than in the TS leading to 1B4R, changing from 2.57 Å (co-adsorption state) to 1.65 Å (Fig. 3b). When the C—H bond begins to form, the Pd—C bond is elongated from 2.17 Å, in the initial state, to 2.38 Å in the TS. Although the C—H bond is being formed and the Pd—C bond is not stretched enough, the activated complex still preserves planarity.

Fig. 4 shows the reaction pathways of the 13BD partial hydrogenation on Pd/Ni(1 1 1), through 1B4R and 2B1R intermediates. The activation barriers to overpass these two TS are 1.14 eV for 1B4R and 0.89 eV for 2B1R, while the transition state energies are 0.88 eV and 0.65 eV, respectively. Furthermore, for this surface the first step through 1B4R radical is slightly exothermic (0.18 eV), whereas for 2B1R intermediate is greatly an exothermic process (0.55 eV). This behavior can be explained considering the higher stability of this radical due to their allylic character (E_{rel} = −0.96 eV for 1B4R with respect to −1.35 eV for 2B1R). Taking into account these results and the Hammond–Leffler postulate [37,38], we would expect early geometries for both TS leading to 1B4R and 2B1R intermediates, i.e. the geometry of these TS would be more similar to that of the co-adsorbed reactive species 13BD and H. Moreover, the TS structure just before 2B1R radical would be even more early geometry than that before 1B4R. This fact can be corroborated making the difference between the initial state (co-adsorption) and the TS

Table 2
Relative reaction energies (E_{rel}) and lateral interaction energies (ΔE_{int}), expressed in eV, of C_4H_x (x = 6 and 7) species co-adsorbed with H on Pd/Ni(1 1 1) and on Pd_3/Ni(1 1 1) surfaces.

Co-adsorption (near to C_x)*	Pd/Ni(1 1 1)		Pd_3/Ni(1 1 1)	
	E_{rel}	ΔE_{int}	E_{rel}	ΔE_{int}
13BD + H (C_1)	−0.80	0.24	−1.36	0.17
13BD + H (C_3)	−0.78	0.26	−1.36	0.17
1B4R + H (C_1)	−0.82	0.14	−0.73	0.11
1B4R + H (C_4)	−0.70	0.26	−0.64	0.20
2B1R + H (C_1)	−1.34	0.01	−0.97	0.19
2B1R + H (C_2)	−1.24	0.11	−0.90	0.26
2B1R + H (C_3)	−1.23	0.12	−0.80	0.36

* C_x corresponds to the carbon atom nearly to the co-adsorbed hydrogen.

Table 3
Transition state energies (ΔE_{TS}), expressed in eV, and the more relevant geometric parameters (expressed in Å) of the TS for the 13BD partial hydrogenation on Pd/Ni(1 1 1) and Pd_3/Ni(1 1 1). In *italic*, the difference values of each distance with respect to the initial state (co-adsorption).

Transition state	Pd/Ni(1 1 1)				Pd_3/Ni(1 1 1)			
	ΔE_{TS}	Pd—H	C—H	Pd—C	ΔE_{TS}	Pd—H	C—H	Pd—C
13BD + H → 1B4R	0.88	1.63	1.68	2.82	1.18	1.60	1.68	2.54
		−0.32	*−1.08*	*0.27*		*−0.28*	*−1.17*	*0.23*
13BD + H → 2B1R	0.65	1.63	1.65	2.38	1.00	1.60	1.64	2.35
		−0.24	*−0.92*	*0.20*		*−0.28*	*−1.01*	*0.22*
1B4R + H → B13R	0.87	1.59	1.66	2.41	1.04	1.60	1.66	2.42
		−0.22	*−1.08*	*0.26*		*−0.27*	*−1.10*	*0.26*
1B4R + H → 1B	0.60	1.60	1.62	2.27	0.76	1.62	1.50	2.27
		−0.31	*−0.95*	*0.20*		*−0.40*	*−0.96*	*0.19*
2B1R + H → 2B	0.60	1.66	1.59	2.24	0.67	1.79	1.50	2.34
		−0.13	*−1.09*	*0.11*		*−0.10*	*−1.10*	*0.21*
2B1R + H → B13R	1.01	1.67	1.57	3.09	1.22	1.59	1.67	2.88
		−0.20	*−1.53*	*0.01*		*−0.25*	*−1.52*	*0.13*
2B1R + H → 1B	0.69	1.65	1.74	2.29	0.80	1.69	1.61	2.29
		−0.14	*−0.86*	*0.11*		*−0.15*	*−0.90*	*0.08*

structure for each relevant distance (Table 2). We observe that these differences for Pd—H, C—H and Pd—C bonds in the TS geometry to the 2B1R radical are smaller in magnitude (0.24 Å, 0.92 Å and 0.20 Å, respectively) than in the TS toward the 1B4R intermediate (0.32 Å, 1.08 Å and 0.27 Å, respectively), according to an early TS structure.

Although the TS complex cannot be experimentally isolated nor directly observed, the corresponding pLDOS (partial local density of states) analyses of the first two activated complexes were performed to give a picture of the main electronic interactions between the TS species and the substrate. Among the different factors that could influence the TS geometry such as the Pd—H, C—H and Pd—C distances, we realize that the influence of the Pd—C distance is the most significant. On Pd/Ni(1 1 1), the C—H and Pd—H distances are very similar in both TS geometries (see Table 3), while the Pd—C distance in the TS structure of 2B1R is 0.44 Å lower than the corresponding TS of 1B4R radical. Therefore, the electronic structure of the interacting C and Pd atoms will reflect this behavior. Similar results were found on Pd_3/Ni(1 1 1) with a shortening of 0.19 Å in the Pd—C distance (shown in the next section). The interacting

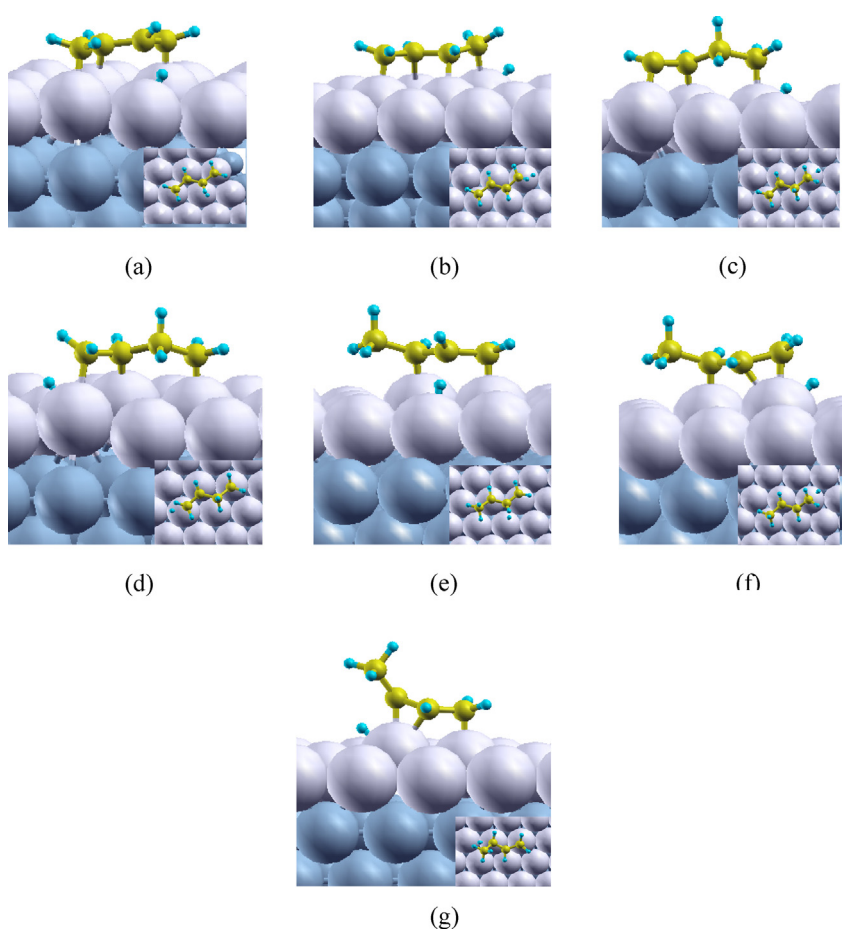

Fig. 3. Transition state structures of the 13BD partial hydrogenation on Pd/Ni(1 1 1), from (a) 13BD to 1B4R, (b) 13BD to 2B1R, (c) 1B4R to 1B, (d) 1B4R to B13R, (e) 2B1R to B13R, (f) 2B1R to 2B and (g) 2B1R to1B.

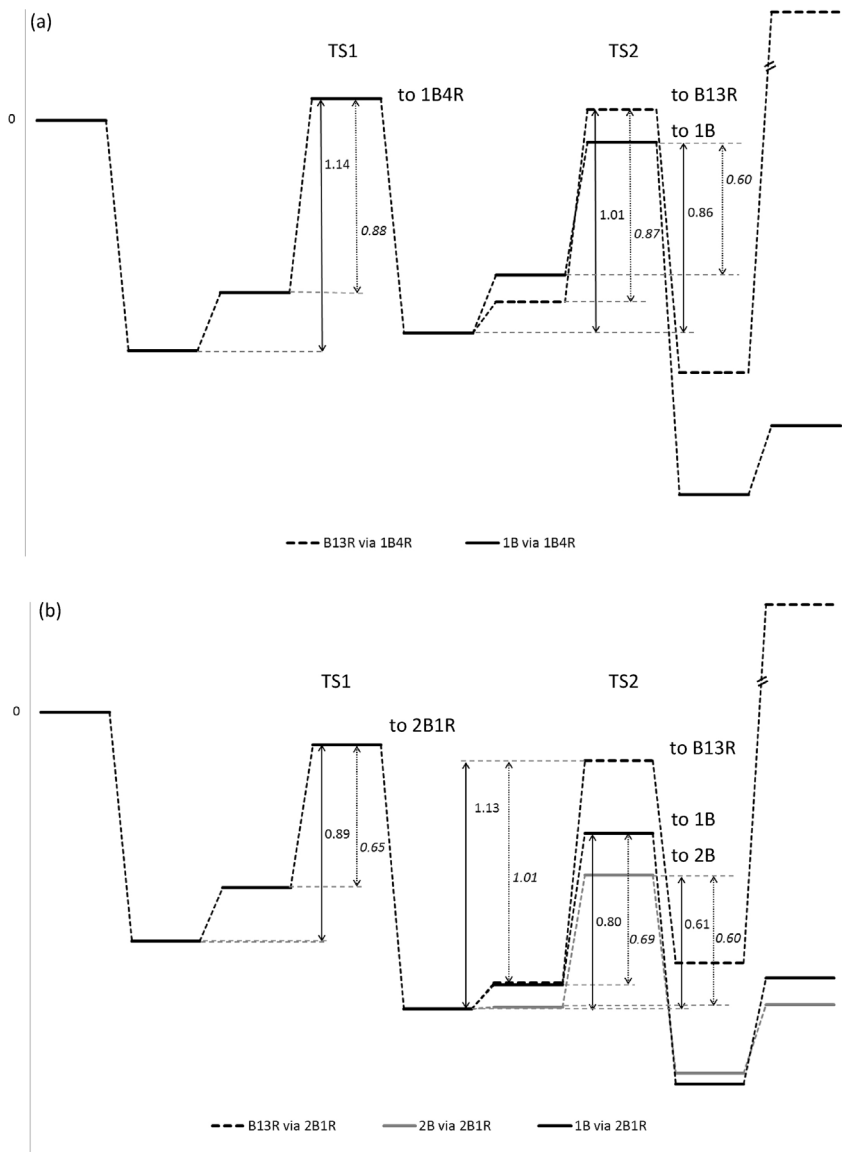

Fig. 4. 13BD hydrogenation energy profiles on Pd/Ni(1 1 1) following through: (a) 1-buten-4-yl (1B4R) and (b) 2-buten-1-yl (2B1R) intermediates. In *italic* the values of transition state energies (ΔE_{TS}) are shown.

orbitals are mainly p_z of C atom and d_{z^2} of Pd atom (Fig. 5). In the TS complex leading to 2B1R (Fig. 5a), there are more electronic states near the Fermi level (taken as energy zero) than in the TS toward 1B4R (Fig. 5b). The interacting orbitals present splitting during all the energy range evaluated, but it is especially stronger between −7.0 eV and −4.0 eV, where the Cp_z orbital of TS complex to the 2B1R intermediate has higher amount of states than the TS to 1B4R. This fact can be related to the lower Pd—C distance in the first activated complex with respect to the 1B4R radical (see Table 2). For this reason, the peak at −7.0 eV is higher in the TS via 1B4R intermediate than in 2B1R ones.

The second step of hydrogenation is more complex because the new H atom can be added in three different positions giving the products B13R, 1B and 2B (see Fig. 4). In case of the 1B4R pathway, two products (B13R and 1B) are only expected. In the activated complex toward 1B product (Fig. 3c), C—H and Pd—C distances are shorter (1.62 Å and 2.27 Å) than for the TS leading to the B13R diradical (Fig. 3d), where distances are 1.66 Å and 2.41 Å, respectively. The activation barriers are of 1.01 eV to obtain B13R and 0.86 eV to give the 1B product and their corresponding TS energies are 0.87 eV and 0.60 eV, respectively. Furthermore, the 1B formation is a more strongly exothermic process than that for B13R (−0.73 eV vs. −0.18 eV), which is in agreement with the fact that the former is more early TS structure than the latter.

If the hydrogenation process occurs through 2B1R intermediate, the products formed are B13R, 1B and 2B. Again, the process to produce B13R would be the pathway requiring more energy (1.13 eV), in which case the TS geometry has the C—H, Pd—H and Pd—C distances of 1.57 Å, 1.67 Å and 3.09 Å, respectively, indicating a later TS structure nature (Fig. 3e). On the other hand, the respective hydrogenations to form the butene isomers require lower activation energies than for B13R; moreover, it is even slightly smaller to obtain the 2B product (0.61 eV for the 2B and 0.80 eV for the 1B). In both cases, TS geometries are early structures because the Pd—C bonds are not much lengthened, showing yet the great interaction with the surface (see Fig. 3f and g). We observe a slight stretch of Pd—C bond from 2.13 Å, in the 2B1R and H co-adsorption, to 2.24 Å, in the TS geometry, to obtain the 2B product. Similar behavior was found for 1B, where the Pd—C bond is elongated from 2.18 Å to 2.29 Å, despite the fact that, after C atom hydrogenation, their

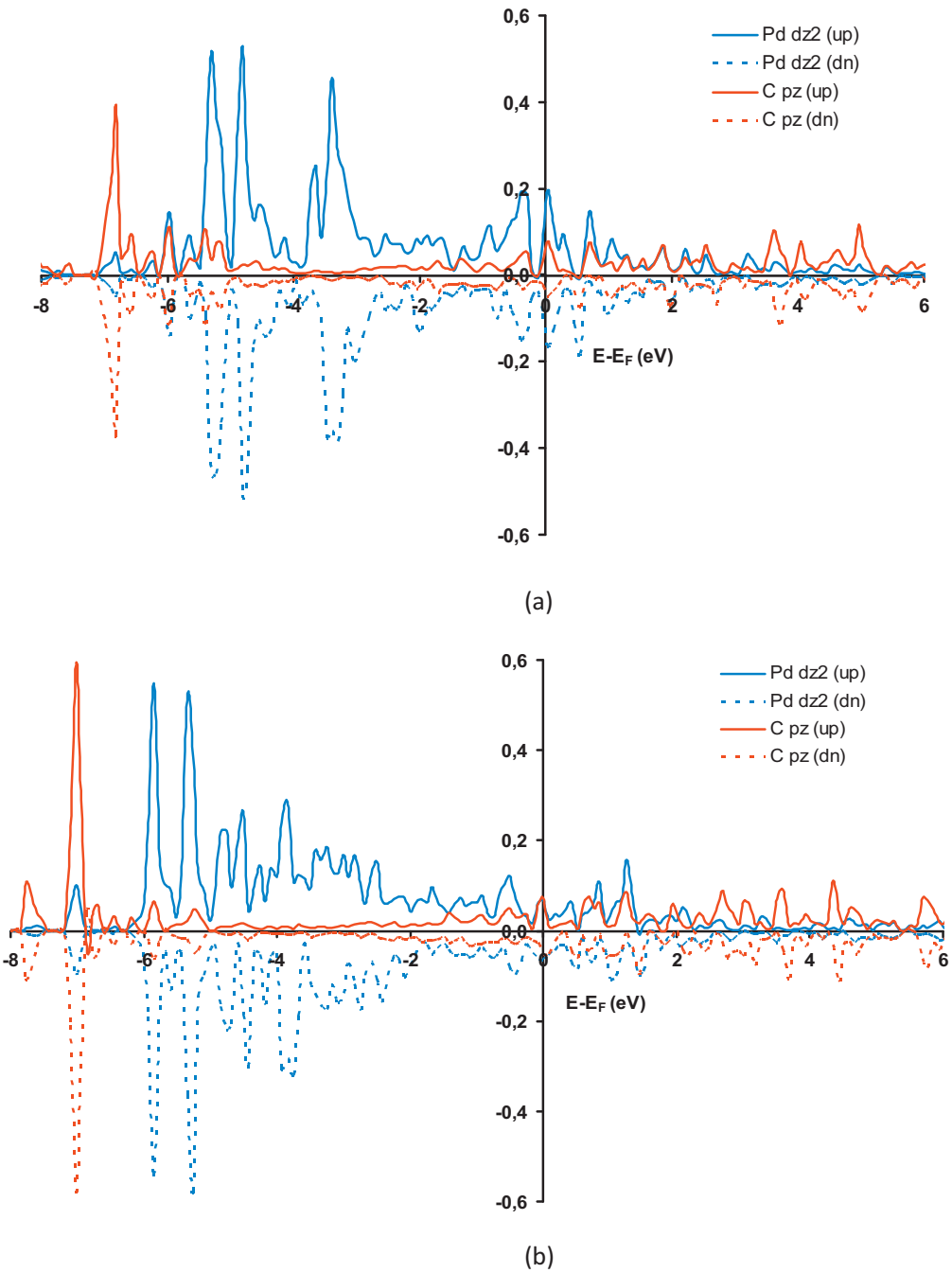

Fig. 5. Partial density of states (pDOS) for TS complexes of the first step of the hydrogenation on Pd/Ni(1 1 1): (a) 13BD + H → 2B1R and (b) 13BD + H → 1B4R. Legend (up) and (dn) correspond to *spin-up* and *spin-down*, respectively.

separation is complete from the metallic surface due to the formation of the methyl group (Pd—C = 5.43 Å).

Comparing both pathways, we can infer that the 13BD hydrogenation process on a Pd/Ni(1 1 1) surface could occur mainly through 2B1R intermediate rather than through 1B4R, because of the lower activation barrier to climb leading to 2B1R. The diradical B13R has the higher activation barriers through both intermediates (1.01 eV via 1B4R and 1.13 eV via 2B1R). For this reason, we could discard the B13R formation on this Pd–Ni surface. Despite this, notice that in the reaction paths showed in Fig. 4, B13R diradical is extremely unstable as a gas phase species; thus, its subsequent hydrogenation forming the butane product would be more feasible. 1B and 2B products are energetically favored with a difference in the activation barriers and energetic stabilities (0.19 eV and 0.05 eV, respectively). The transition state energies of 1B and 2B isomers are very similar (with a difference of 0.09 eV). Taking into account this slight difference, it is possible to conclude that both butene isomers are equally probable. These results indicate that the 13BD partial hydrogenation on Pd/Ni(1 1 1) occurs with some degree of butene selectivity without the production of butane, contrary to the case of a Pt(1 1 1) catalyst [30]. Considering that hydrogenation takes place via 2B1R intermediate, B13R formation requires an extremely high TS energy to be overcome, in contrast to the butene isomers. Comparing this surface with pure Pd catalyst [30], we note the high

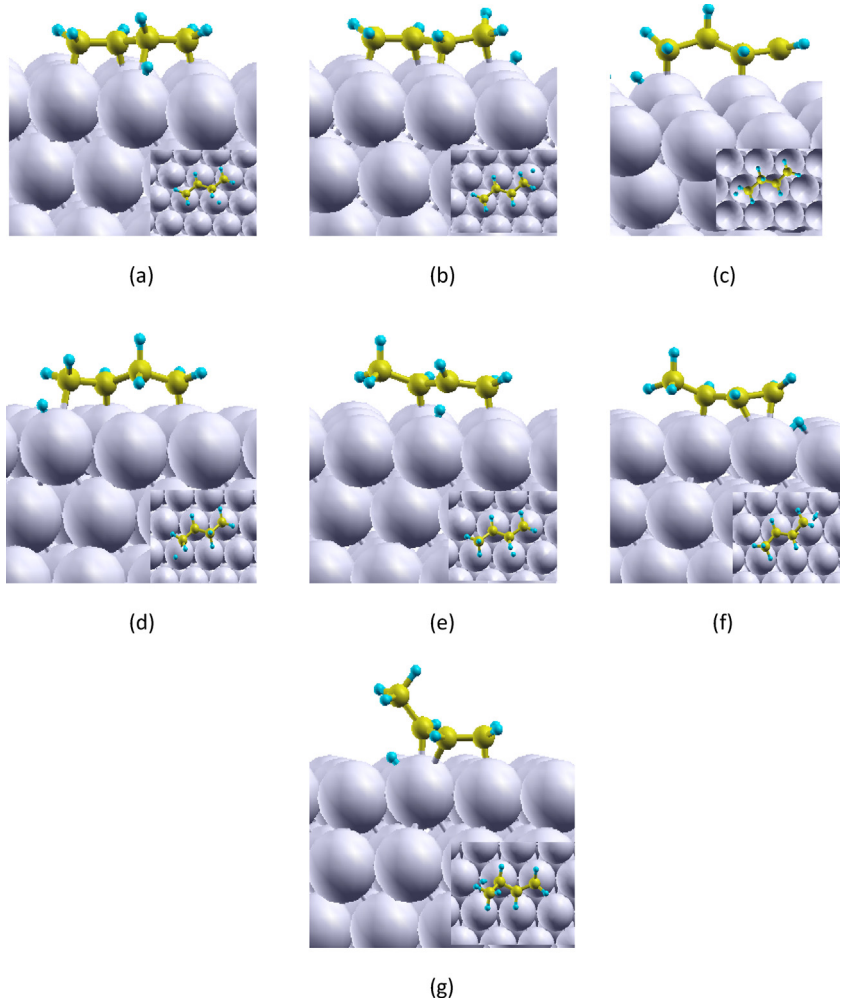

Fig. 6. Transition state structures of the 13BD partial hydrogenation on Pd_3/Ni(1 1 1): from (a) 13BD to 1B4R, (b) 13BD to 2B1R, (c) 1B4R to 1B, (d) 1B4R to B13R, (e) 2B1R to B13R, (f) 2B1R to 2B and (g) 2B1R to1B.

activity of Pd/Ni(1 1 1) and the fact that both surfaces will produce similarly products with a slight selectivity leading to 2B on Pd–Ni surface.

3.3.2. *On Pd_3/Ni(1 1 1)*

This surface has similar electronic and structural characteristics to the pure Pd(1 1 1) [17]; however, in the 13BD partial hydrogenation pathway there are some differences that will be discussed in this subsection. It is worth remembering that, in general, the changes undergone by the three bonds characterizing the TS structure, C—H, C—Pd and Pd—H, provide the type of TS geometry; the greater the variation of these bonds, the more like a late TS geometry would be. This behavior will be observed in a greater extent on the Pd_3/Ni(1 1 1) surface, due to their more endothermic steps with respect to Pd/Ni(1 1 1).

In the first steps of the 13BD hydrogenation on Pd_3/Ni(1 1 1), the TS geometries leading to the radicals 1B4R (Fig. 6a) and 2B1R (Fig. 6b) are similar to their corresponding structures obtained on Pd/Ni(1 1 1) (Table 3). The most significant difference takes place in Pd—C distances. Nevertheless, the variations of these distances show the true bond modification. The C—H bond changes are higher for TS on Pd_3/Ni(1 1 1) than on Pd/Ni(1 1 1); it can be visualized by means of the difference between the TS geometry and that of the previous co-adsorption situation (see also *italic* font in Table 3). Therefore, the TS geometrical configuration is in agreement with a later structure. Besides, the TS energies are noteworthy higher on Pd_3/Ni(1 1 1) than on Pd/Ni(1 1 1); the first step to 1B4R on Pd_3/Ni(1 1 1) is a thermodynamically less favorable process, whereas the step through 2B1R changes from exothermic on Pd/Ni(1 1 1) to endothermic on Pd_3/Ni(1 1 1) (Fig. 7). Again, the TS energy leading to the 1B4R radical requires higher energetic cost than to 2B1R radical. The energy difference to obtain 1B4R with respect to 2B1R is lower on Pd_3/Ni(1 1 1) than on Pd/Ni(1 1 1) surface.

The optimized TS geometries for the second step of 13BD hydrogenation are also shown in Fig. 6c–g. Through both intermediates, B13R formation is an endothermic process with the highest activation barrier of all the products, being more hindered through the 2B1R intermediate pathway. On the other hand, the steps to the 1B and 2B products are exothermic and slightly endothermic processes, respectively. However, taking into account the activation energies of these steps, we observe the same tendency previously obtained on Pd/Ni(1 1 1). That is, the energy was lower for 2B than for 1B, but the requirement to overcome the activation barriers for the corresponding TS on Pd_3/Ni(1 1 1) are higher than on Pd/Ni(1 1 1). The butene isomers present a greater energy difference in the transition state energies on Pd_3/Ni(1 1 1) with respect to Pd/Ni(1 1 1) (0.13 eV vs. 0.09 eV).

As it was observed on previously reported Pd(1 1 1) [30], almost all the steps in 13BD hydrogenation on Pd_3/Ni(1 1 1) are endothermic processes, except in the 1B formation through 1B4R monoradical. The only difference between these surfaces was

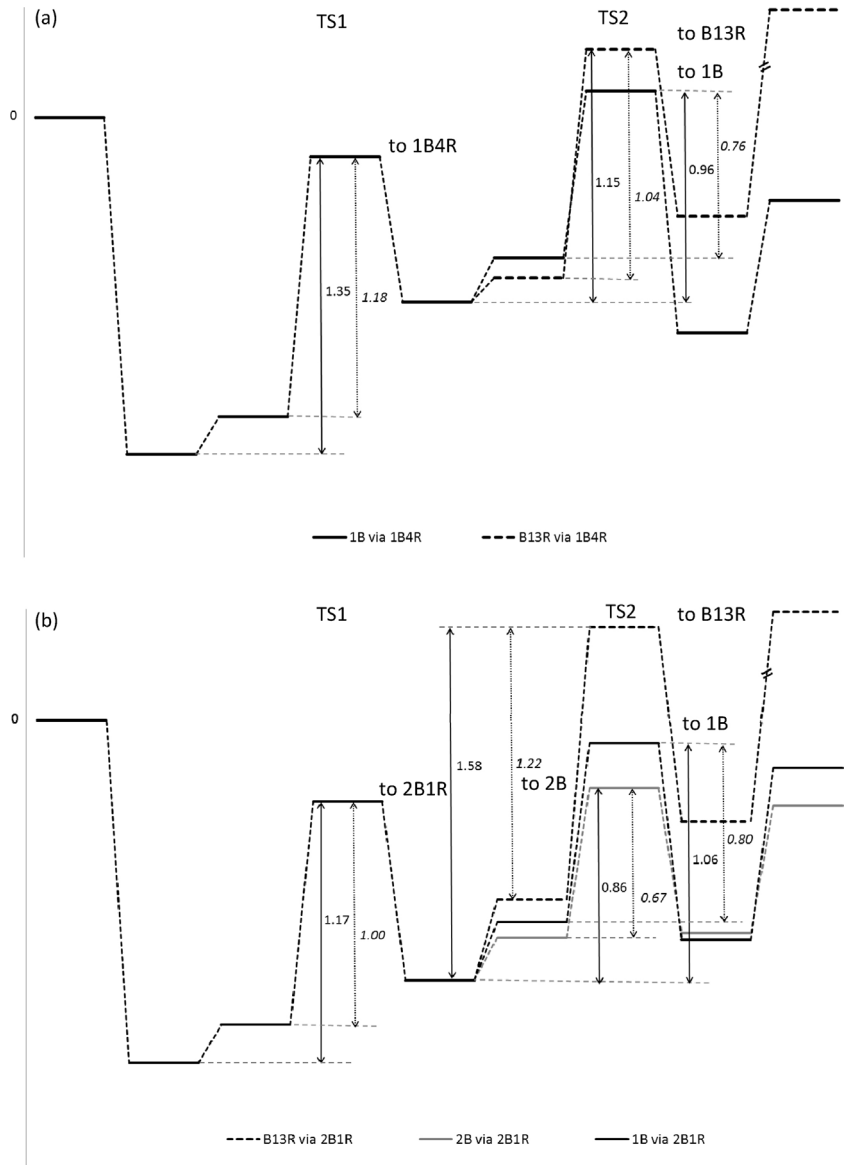

Fig. 7. 13BD hydrogenation energy profiles on Pd_3/Ni(1 1 1) following through: (a) 1-buten-4-yl (1B4R) and (b) 2-buten-1-yl (2B1R) intermediates. In *italic* the values of transition state energies (ΔE_{TS}) are shown.

obtained for the 1B product through the 2B1R intermediate, where this step is slightly exothermic on Pd_3/Ni(1 1 1). On the other hand, although the activation energies were not improved on Pd_3/Ni(1 1 1) with respect to the pure Pd(1 1 1), it would be expected that the selectivity to 2B formation should be favored. Indeed, using the activation energies from Figs. 4 and 7 together with the results reported by Sautet et al. [30], and considering the relative probability to obtain 2B versus 1B by means of the corresponding Boltzmann's factor at 300 K (neglecting pre-exponential entropic factors), the 2B/1B ratio should be much bigger for the Pd_3/Ni(1 1 1) system than for Pd(1 1 1). This probability is also improved on Pd/Ni(1 1 1) with respect to the pure Pd(1 1 1) [30], but in a smaller magnitude than on the system Pd_3/Ni(1 1 1). Besides, the TS energy of the B13R is even higher on Pd_3/Ni(1 1 1) than on Pd(1 1 1), compared to butenes. For the first steps of the overall reaction, the TS geometries on Pd_3/Ni(1 1 1) have the Pd–H distances lower and the C—H and Pd—C bonds larger than the corresponding TS bonds on Pd(1 1 1). These characteristics indicate that the TS structures are earlier on Pd_3/Ni(1 1 1) than on Pd(1 1 1).

Partial Local Density of States (pLDOS) of the TS structures toward 2B1R and 1B4R radicals on Pd_3/Ni(1 1 1) are shown in Fig. 8. Comparing these profiles with the corresponding structures on Pd/Ni(1 1 1), we note that the coupling between Cp_z orbital and Pd d-band is most significant on Pd/Ni(1 1 1). In the energy interval of most relevant overlapping between the C p-band and Pd d-band, a small number of Cp_z states localized in the range from −6.0 eV to −4.0 eV was observed. Besides, the peaks at −7.0 eV corresponding to Cp_z orbital are even lower in the TS structures on Pd_3/Ni(1 1 1). All the results are consistent with the lower stabilities of the activated complexes on Pd_3/Ni(1 1 1) than on Pd/Ni(1 1 1).

Considering the reaction pathways evaluated, we highlight that the 13BD hydrogenation is a more favorable process on Pd/Ni(1 1 1) surface compared to Pd_3/Ni(1 1 1), due to the lower activation energies, despite the stronger stabilization of the initial adsorbed state (13BD and H independently adsorbed) on Pd_3/Ni(1 1 1) in comparison with Pd/Ni(1 1 1). Similar results were obtained by other authors for ethanol dehydrogenation on Pt(1 1 1), with respect to its respective hydrated surface [39]. Besides, the reaction proceeds through the 2B1R intermediate, giving the butene isomers

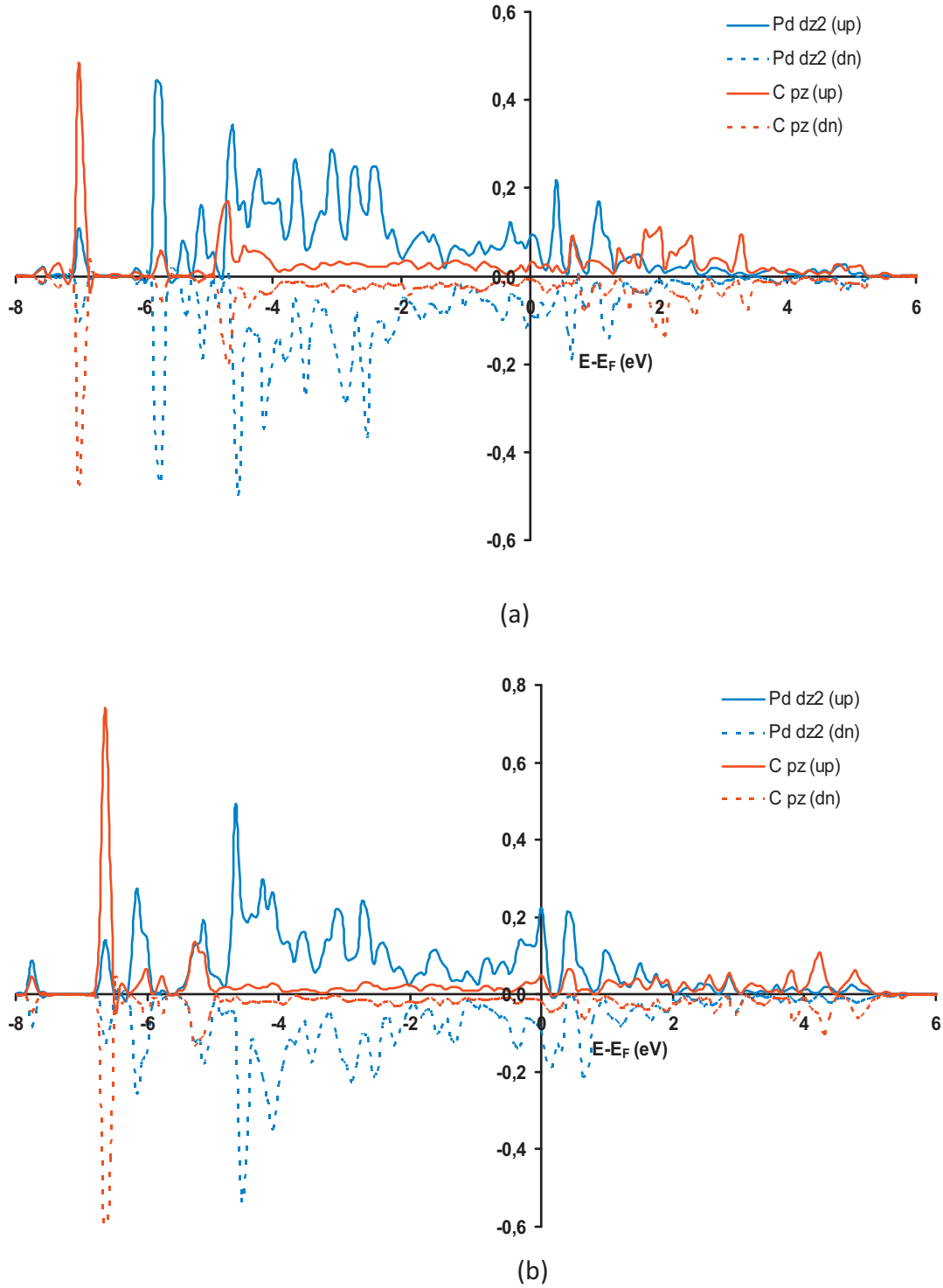

Fig. 8. Partial density of states (pDOS) for TS complexes of the first step of the hydrogenation on Pd_3/Ni(1 1 1): (a) 13BD + H → 2B1R and (b) 13BD + H → 1B4R. Legend (up) and (dn) correspond to *spin-up* and *spin-down*, respectively.

as the main products. The selectivity to 2B instead of 1B isomers is enhanced on Pd/Ni(1 1 1) surface compared to Pd(1 1 1), and highly favored with respect to the B13R product. Then, the formed butene isomers desorbs from the surface while the 13BD is present in gas phase, because their adsorption energy is highly favored with respect to butenes (−0.16 eV vs. −0.52 eV, respectively). From these results and taking into account the activated energies to form 1B and 2B products, we would expect higher activity and selectivity to 2B instead of 1B on Pd/Ni(1 1 1), and very low or negligible butane production, the last coming from the subsequent B13R hydrogenation, with respect to Pd(1 1 1) [30].

Our calculations predict that the Pd/Ni(1 1 1) catalyst model would improve the activity and the selectivity toward the 2B product, compared to the Pd(1 1 1) surface. Experimental results obtained by Bertolini [40] showed that the chemisorptive properties of Ni(1 1 1) and Ni(1 1 0) surfaces can be modified depositing another metal with a greater atomic radius like Pd and Pt. This author also demonstrated that the catalytic activities of the

Pd–Ni(1 1 1) catalysts have a selectivity toward butenes of 100%, up to complete 13BD conversion. This behavior is due to the strain suffered by the surface atoms that modifies their electronic properties.

At the present, we are investigating the hydrogenation pathway starting from the 13BD adsorbed in the di-π-*cis* mode to give the *cis*-2B isomer, at variance with the reaction studied in this work, where the 2B obtained from the 13BD adsorbed in the 1,2,3,4-tetra-σ mode is the *trans*-2B isomer. It is important to highlight that the 13BD adsorbed on di-π-*cis* site of Pd/Ni(1 1 1) is only 0.1 eV less stable than the 1,2,3,4-tetra-σ site on the same surface. [18].

4. Conclusions

Partial hydrogenations of 13BD on both bimetallic surfaces were evaluated following the Horiuti–Polanyi mechanism. The whole process was found to be exothermic on Pd/Ni(1 1 1), where the intermediate adsorptions are more favorable exhibiting lower activation barriers than on Pd_3/Ni(1 1 1). The pathway through the 2B1R intermediate turned out to be the most favorable on both surfaces too, compared to the 1B4R radical. On Pd/Ni(1 1 1) and Pd_3/Ni(1 1 1), the B13R formation is associated with high activation barriers through both pathways studied here; for this reason, it is extremely improbable to obtain B13R. Interestingly, this process is even more unlikely via the pathway with lower thermodynamic requirement. The products would be mainly the butene isomers, with an enhancement of the selectivity toward 2B, in contrast to the pure Pd surface and in agreement with experimental data.

From these results it is possible to observe that the most strained Pd atoms of the Pd/Ni(1 1 1) catalyst model suffer an important modification of their electronic properties, varying the intermediates stabilization and the transition states. These conclusions also agree with experiments.

Acknowledgements

The authors thank the financial support from the Consejo Nacional de Investigaciones Científicas y Técnicas (CONICET) (Grant No. PIP 2009 – N°112-200801-02286), the Agencia de Promoción Científica y Tecnológica (ANPCyT) (Grant No. PICT 2010 - N° 0830) and the Universidad Nacional del Sur (UNS) (Grant No. PGI – UNS N° 24/F051).

References

[1] D. Seth, A. Sarkar, F.T.T. Ng, G.L. Rempel, Chem. Eng. Sci. 62 (2007) 4544–4557.
[2] Y. Okamoto, K. Fukino, T. Imanaka, S. Teranishi, J. Catal. 74 (1982) 173–182.
[3] P. Hermann, J.M. Guigner, B. Tardy, Y. Jugnet, D. Simon, J.C. Bertolini, J. Catal. 163 (1996) 169–175.
[4] E.S. Jang, M.Y. Jung, D.B. Min, Compr. Rev. Food Sci. Food Saf. 4 (2005) 22–30.
[5] F.E. Scarbrough, Am. J. Clin. Nutr. 65 (1997) 1578S–1580S.
[6] Y.Y. Yeo, A. Stuck, C.E. Wartnaby, D.A. King, Chem. Phys. Lett. 259 (1996) 28–36.
[7] Q. Ge, D.A. King, J. Chem. Phys. 110 (1999) 4699–4702.
[8] J. Silvestre-Albero, G. Rupprechter, H-J. Freund, Chem. Commun. (2006) 80–82.
[9] P. Sautet, J.-F. Paul, Catal. Lett. 9 (1991) 245–260.
[10] A. Valcarcel, A. Clotet, J.M. Ricart, F. Delbecq, P. Sautet, Surf. Sci. 549 (2004) 121–133.
[11] P.A. Sheth, M. Neurock, C.M. Smith, J. Phys. Chem. B 107 (2003) 2009–2017.
[12] M. Neurock, R.A. van Santen, J. Phys. Chem. B 104 (2000) 11127–11145.
[13] V. Pallassana, M. Neurock, J. Catal. 191 (2000) 301–317.
[14] I. Lee, F. Zaera, J. Am. Chem. Soc. 127 (2005) 12174–12175.
[15] I. Lee, R. Morales, M.A. Albiter, F. Zaera, PNAS 105 (2008) 15241–15246.
[16] P. Hermann, B. Tardy, D. Simon, J.M. Guigner, B. Bigot, J.C. Bertolini, Surf. Sci. 307–309 (1994) 422–427.
[17] G. Gómez, G.F. Cabeza, P.G. Belelli, J. Magn. Magn. Mater. 321 (2009) 3478–3482.
[18] G. Gómez, P.G. Belelli, G.F. Cabeza, N.J. Castellani, J. Solid State Chem. 183 (2010) 3086–3092.
[19] G. Kresse, J. Hafner, Phys. Rev. B: Condens. Matter 47 (1993) 558–561.
[20] G. Kresse, J. Hafner, Phys. Rev. B: Condens. Matter 48 (1993) 13115–13118.
[21] G. Kresse, J. Hafner, Phys. Rev. B: Condens. Matter 49 (1994) 14251–14269.
[22] J.P. Perdew, J.A. Chevary, S.H. Vosko, K.A. Jackson, M.R. Pederson, D.J. Singh, C. Fiolhais, Phys. Rev. B: Condens. Matter 46 (1992) 6671–6687.
[23] J.P. Perdew, J.A. Chevary, S.H. Vosko, K.A. Jackson, M.R. Pederson, D.J. Singh, C. Fiolhais, Phys. Rev. B: Condens. Matter 48 (1993) 4978.
[24] P. Blochl, Phys. Rev. B: Condens. Matter 50 (1994) 17953–17979.
[25] G. Kresse, D. Joubert, Phys. Rev. B: Condens. Matter 59 (1999) 1758–1775.
[26] M. Methfessel, A.T. Paxton, Phys. Rev. B: Condens. Matter 40 (1989) 3616–3621.
[27] J. Horiuti, M. Polanyi, Trans. Faraday Soc. 30 (1934) 1164–1172.
[28] J. Horiuti, M. Polanyi, J. Mol. Catal. A: Chem. 199 (2003) 185–197.
[29] H. Jónsson, G. Mills, K.W. Jacobsen, in: B.J. Berne, G. Ciccotti, D.F. Coker (Eds.), Classical and Quantum Dynamics in Condensed Phase Simulations, World Scientific, Singapore, 1998.
[30] A. Valcárcel, A. Clotet, J.M. Ricart, F. Delbecq, P. Sautet, J. Phys. Chem. B 109 (2005) 14175–14182.
[31] W. Eberhardt, S.G. Louie, E.W. Plummer, Phys. Rev. B: Condens. Matter 28 (1993) 465–477.
[32] V. Pallassana, M. Neurock, L.B. Hansen, B. Hammer, J.K. Norskov, Phys. Rev. B: Condens. Matter 60 (1999) 6146–6154.
[33] M. Pérez Jigato, B. Coussens, D.A. King, J. Chem. Phys. 118 (2003) 5623–5634.
[34] J. Greeley, M. Mavrikakis, J. Phys. Chem. B 109 (2005) 3460–3471 (and references therein).
[35] J.-F. Paul, P. Sautet, Phys. Rev. B: Condens. Matter 53 (1996) 8015–8027.
[36] P. Légaré, Surf. Sci. 559 (2004) 169–178.
[37] G.S. Hammond, J. Am. Chem. Soc. 77 (1955) 334–338.
[38] J.E. Leffler, Science 117 (1953) 340–341.
[39] D. Loffreda, C. Michel, F. Delbecq, P. Sautet, J. Catal. 308 (2013) 374–385.
[40] J.C. Bertolini, Appl. Catal., A: Gen. 191 (2000) 15–21.